Biomedical Signal Processing and Control 71 (2022) 103160

Contents lists available at ScienceDirect

Biomedical Signal Processing and Control

journal homepage: www.elsevier.com/locate/bspc

Skin cancer detection using Kernel Fuzzy C-means and Developed Red Fox Optimization algorithm

Zexian Fu [a], Jing An [a], Qiuyu Yang [a], Haojun Yuan [a], Yuhang Sun [a,*], Homayoun Ebrahimian [b]

[a] Affiliated Hospital of Hebei University of Engineering, Handan City, Hebei 056002, China
[b] Department of Engineering, Ardabil Branch, Islamic Azad University, Ardabil, Iran

ARTICLE INFO

Keywords:
Melanoma diagnosis
Gray-level co-occurrence matrix
Developed Red Fox Optimization (DRFO) Algorithm
Kernel Fuzzy C-means
Multi-layer perceptron

ABSTRACT

The present study provides an optimal pipeline methodology for the accurate diagnosis of melanoma from dermoscopy images. Here, after image preprocessing, the region of interest is segmented by a method based on the Kernel Fuzzy C-means method. Afterward, the main characteristics of the segmented area have been optimally extracted and selected based on a new optimized algorithm. Finally, an optimized classification methodology based on multi-layer perceptron is proposed for the final diagnosis. The optimization of feature selection and classification is accomplished by a newly developed version of the Red Fox Optimization (DRFO) Algorithm to provide a result with higher accuracy and reliability. Simulations are applied to the ISIC 2020 database concerning some performance indexes and are compared with the results and some famous approaches to demonstrate the effectiveness of the method toward the others.

1. Introduction

One of the most usual diseases is cancer that has affected many people around the world [1]. The term cancer refers to a large family of diseases that involve the abnormal growth of cells, and these cells have the ability for spreading to other parts of the body and attack it [2]. During this disease, a subset of neoplasms form; A neoplasm or tumor is a group of cells that have grown during an uncontrollable growth and usually eventually form a mass, but this mass can spread throughout the body [3]. Cancer is the most common type of cancer [4]. Skin cancers are malignant tumors in which there is uncontrolled proliferation of skin cell types, while the natural process of skin regeneration involves the proliferation of cells in a controlled manner [1]. Each specific type of skin cancer has unique characteristics. Most skin cancers localize the cancerous growth (malignancy) of the skin [5].

They originate from the cells of the epidermis, the surface layer of the skin. Unlike malignant melanoma of the skin, the vast majority of these skin cancers rarely spread (metastasize) to other parts of the body and become life-threatening [6]. One of the most dangerous kinds of skin cancer involves the cells (melanocytes) which generate melanin. Melanoma is created in the eyes and rarely inside your body, such as your nose or throat [7]. The exact cause of melanoma is not known, but exposure to the sun's ultraviolet rays or tanning lamps increases the risk of skin cancer [8,9]. Less exposure to the sun could help to decrease the risk of skin cancer. Skin cancer risk is growing in people under forty, particularly women. Recognizing the skin cancer symptoms could help you diagnose cancer early. If diagnosed early, melanoma can be successfully treated.

A skin cancer diagnosis is a difficult task due to the appearance of different types of skin lesions, especially Melanoma and Nevi. Even with dermoscopy, a non-invasive testing technique, the accuracy of melanoma diagnosis by dermatologists is 75% to 84%. To prevent unnecessary biopsy, researchers have reviewed several non-invasive methods for diagnosing melanoma. These methods usually consist of three steps: boundary segmentation, features extraction, and classification. Based on the Cancer Cell Organization, in 2019, Melanoma cancer with 15,000 cases is the fourth most common cancer in the world. Also, based on this organization, Melanoma is the 9th most common reason for cancer death in 2019 [10].

There are several types of research works that study different parts of medical imaging for Melanoma. For example, Somfai et al. [11] suggested s machine vision system for melanoma detection. The paper introduced a diagnosis system based on deep learning to provide an accurate method with less value of the false-negative rate. The method was used based on using a U-net CNN for automatic segmentation of the melanoma. The features of the segmented images were then extracted.

* Corresponding author.
E-mail address: drsyh18031023658@163.com (Y. Sun).

https://doi.org/10.1016/j.bspc.2021.103160
Received 31 March 2021; Received in revised form 23 August 2021; Accepted 7 September 2021
Available online 28 September 2021

The features are then processed by tailored neural networks. The results indicated advancement in all parts through a baseline.

Bansal et al. [12] presented a method of melanoma detection based on a deep learning-based image feature extraction. The feature extraction in the study was performed by the Convolutional Neural Network (CNN) based on transfer learning and a pipeline classifier including random forest (RF), k-nearest neighbor (KNN), and AdaBoost to classify the melanoma based on the extracted features from the CNN. Simulation results indicated suitable efficiency for the proposed method.

Fan et al. [13] used spatial features and spectral features to simplify the melanoma detection process from the other materials. The study used a spectral preprocessing technique on the microscopic hyperspectral images to provide a preprocessing method and then it used three supervised classifications including CNN, maximum likelihood classification (MLC), and support vector machine (SVM) to perform the final classification. Simulation results calculated the precision of the classifiers to determine the best classification method.

Vocaturo et al. [14] used Epiluminescence microscopy (ELM) as a new widely-used method for the aim of melanoma detection. The study used the ELM technique to recognize reference features that can be utilized by the new researchers as a beginning point of future works.

Dey et al. [15] introduced an optimized machine vision methodology for melanoma diagnosis. In that study, they used Bat Algorithm to optimize the method and achieve better efficiency for the images. After performing the preprocessing on the images, they were processed with the Distance-Regularized-Level-Set (DRLS) segmentation method, and the efficiency is validated by computing the essential image performance metrics (IPM). Simulation results showed that the method satisfies the final purpose compared with some other methods. Nevertheless, there are still several research gaps to be conducted. Proposing a high accuracy and optimized method for this purpose is still open and needs improvements. Therefore, using proper methods can assist the specialists to diagnose the disease with higher precision. The main idea of this study is to introduce a new optimal pipeline strategy for accurate melanoma detection of dermoscopy images. The main contribution here is to design a newly developed version of Red Fox Optimization (DRFO) for optimal features selection and optimal classification of the system. Also, a specific structure based on Kernel Fuzzy C-means is used for this purpose for segmenting the region of interest from dermoscopy images. Therefore, the main contributions of this study can be highlighted as follows:

- An optimized pipeline method for accurately melanoma detection of dermoscopy images.
- The region of interest is segmented by a method based on Kernel Fuzzy C-means method.
- The main features of the segmented area are extracted.
- The features are reduced based on a new developed version of Red Fox Optimization (DRFO) Algorithm
- An optimized Multi-layer perceptron based on DRFO is proposed for the final diagnosis.
- Simulations are compared applied to the ACS database and compared with some renown approaches

2. Image preprocessing

The first stage in medical image processing for any purpose is to perform some kinds of preprocessing to improve the quality of the original images and to simplify the next stages of operations. The skin images usually include some artifacts such as reflections, hairs, skin lines, air bubbles, and shadows that influence the image segmentation stage. Different methods were introduced for this purpose, like intensity correction, color space transformation, artifact removal, and contrast enhancement. One simple method for improving the quality of images with artifact elimination is to use the median filter. Indeed, this filter can be used for smoothing images, and consequently, it softens the high-frequency artifacts like noise, extra lines, and hair, without losing relevant information about the lesions, and, so it improves the segmentation precision. Median filtering is a nonlinear process that smoothens the images, unlike linear filters with keeping the original image with no edge blurring. This filter may be used for smoothing the skin lesion images, in addition, to remove artifacts, keeping the lesion edges. To provide operative smoothing, the mask size of the median filter should be proportional to the original image. This study uses a 9×9 convolution mask on the images meanwhile other masks did not properly smooth the image with a well level of noise reduction. The middle filter substitutes a pixel by the middle of whole pixels in a vicinity w, i.e.

$$y[m,n] = median(x[i,j],(i,j) \in w) \quad (1)$$

where, w describes a neighborhood defined by the user, centered about location $[m,n]$ in the image.

A median filter's 2D window can be any central symmetric shape, such as a round disc, rectangle, square, or cross. The center pixel will be substituted by the median of all pixel values inside the window. The main operation in this filter is sorting. Several sorting algorithms are introduced for this purpose with complexity ($nlog_2n$). However, in this study, with the limited number of pixels, a simple sorting method is utilized with complexity (n^2). The pseudo-code of this method is given below:

```
for (i = 0; i < n-1; i++)
for (j = i + 1; j < n; j++)
if (bin[i] < \;bin[j]) {
w = bin[i]; bin[i] = bin[j]; bin[j] = w;
}
```

Fig. 1 shows an example of applying preprocessing to an input image.

3. Skin cancer area segmentation based on clustering

Object classification is clustering, therefore objects in the identical group are so near to each other in properties. In recent decades, clustering algorithms have shown remarkable progress in segmentation and image segmentation. Due to its good performance in optimization and simplicity of implementation, optimization algorithms have attracted a lot of interest. Often, the similarity is determined by a distance scale such as the Euclidean distance or the Manhattan distance. Data mining, categorizing stock data and image segmentation are some of the applications of this algorithm. It can be said that image segmentation is the main step in many processing of image processing and machine vision applications.

The result of slicing an image is a set of pieces that make up the whole image or a set of lines extracted from the image (edge recognition). There are general techniques and algorithms for slicing images, and most of these techniques are knowledgeable [16]. The domain is effectively combined to solve the problem of the segmentation of images in a particular subject. The degree of segmentation depends on the subject under consideration, which means that when the user objects are

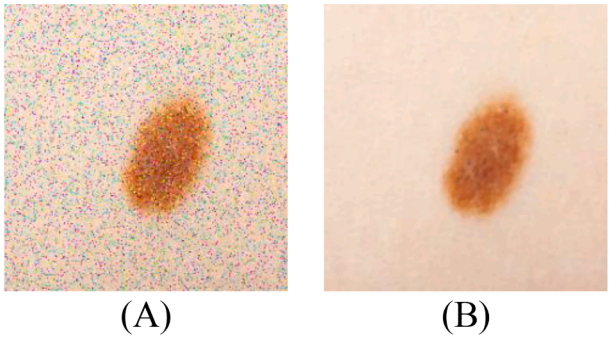

Fig. 1. An example of applying the preprocessing on an input image.

separated, segmentation must be stopped. Because color, texture, and edge achieve the high-level features that humans use in analyzing scenes, categorizing, and recognizing images. The fuzzy C-mean method is one of the clustering methods in image segmentation.

In this study, an improved four-step Fuzzy C-means method is presented for skin cancer area segmentation. The first step is to first produce superpixels using the Simple Linear Iterative Clustering (SLIC) algorithm [17,18]. This algorithm produces superpixels using CIE LAB color space in 5D space. Dissimilar to the RGB and CMYK color spaces, Lab color has been designed for modeling human vision. This color space can be employed to make precise color balance corrections by adjusting the lightness contrast using the components [19]. Then, two categories of color and texture properties of the image are used to index and separate the superpixels and finally to find the parts of the image. In the second stage, the color property of each superpixel is extracted and the color property of each superpixel is arranged in such a way that for each image in HSV space, three separate histograms for S, H, and V channels are considered and for preventing the time complexity, each histogram has been quantized into 8, 4, and 4 sub-distances and in the next step, the NSCT algorithm is used to find the feature of the texture. In the next step, the data generated using the proposed new method of clustering is clustered with a fuzzy core, and all superpixels that have a cluster tag are placed in one segment.

In the proposed method, the new Kernel Fuzzy C-Means (KFCM) algorithm is used for image segmentation. The KFCM provides a central version of FCM that uses a kernel function for calculating the distance of data points from cluster centers. The KFCM algorithm offers an image clustering technique with higher accuracy significantly compared with the classical Fuzzy C-Means algorithm. In practical applications terms of view, it is preferred by researchers and has progressively formed a comprehensive theoretical system over the continuous application and research [20]. Compared with other clustering methods, it gives the best result for overlapped data sets [21]. Also, unlike most clustering methods such as k-means, where data points should completely be owned by one cluster center, here data point is assigned. In KFCM, data is written from the input space to a higher-dimensional space, commonly called the core space, and the data is represented as simpler structures or patterns. The core function in this algorithm is calculated by the following formula:

$$K = \exp\left(-\|x-y\|^2/\rho\right) \tag{2}$$

First, the membership function is calculated, and then, using a kernel fuzzy similarity measure, we calculate the belonging of each data sample to the clusters. The steps of the algorithm used in this research are as follows.

1) The set of objects is first clustered using the KFCM algorithm and a U membership matrix is generated [22].
2) For each element x_i, x_j , the number of t nearest neighbor is found.
3) For all pairs of objects, x_i, x_j, if x_i, x_j are not t nearest neighborhood, $W_{ij} = 0$, else, if they belong to a cluster, $W_{ij} = 1$, otherwise, $W_{ij} = \exp\left(ln2 \times \left(u_i \oplus u_j\right)\right)$, where, $\oplus$ describes the exclusive OR which shows the overlap between two fuzzy sets.
4) In this step, a diagonal matrix, D, is defined that the element $D_{ij}$is equal to the sum of the i^{th} column of matrix W, so,

$$D_{ij} = \sum_{j=1}^{n} W_{ij} \tag{3}$$

Then, it is normalized as follows:

$$L = D^{-1/2} W D^{1/2} \tag{4}$$

The number of K larger eigenvector than L (the first vector) is found (the first vector is selected) and the matrix $P = \left[p^1, p^2, \cdots, p^k\right]$ is formed and then the algorithm normalizes each row in the P matrix

To form matrix Y as follows:

5) Each line of Y is considered a point in space R^k and at the end, the final clustering is done by using the K-mean algorithm.

Fig. 2 shows a sample example for skin cancer using the proposed method.

4. Feature extraction

To improve the system's accuracy and decreasing its complexity, a feature extraction should be performed on the segmented images. Indeed, The task of feature extraction is to extract the features from the image.

Also, using lots of features for processing can increase the complexity of the system. Therefore, a good idea is to just select some useful features and extract them from the segmented images. In this paper, the feature selection has two modes: a selected feature will be marked by 1 whereas the non-selected features will be specified by zero. Because of using 19 features in this study, we have 19 decision variables that should be selected optimally. The present study uses Statistical properties, Geometric properties, and Texture properties for feature extraction. The mathematical formulation for these properties is as follows:

$$Area = \sum_{i=1}^{M}\sum_{j=1}^{N} p(i,j) \tag{5}$$

$$Contrast = \sum_{i=1}^{M}\sum_{j=1}^{N} p^2(i,j) \tag{6}$$

$$Mean = \frac{1}{MN}\sum_{i=1}^{M}\sum_{j=1}^{N} p(i,j) \tag{7}$$

$$Entropy = \sum_{i=1}^{M}\sum_{j=1}^{N} p(i,j)\log p(i,j) \tag{8}$$

$$Rectangularity = \frac{Area}{a \times b} \tag{9}$$

$$Homogeneity = \sum_{i=1}^{M}\sum_{j=1}^{N} \frac{p(i,j)}{1+|i-j|} \tag{10}$$

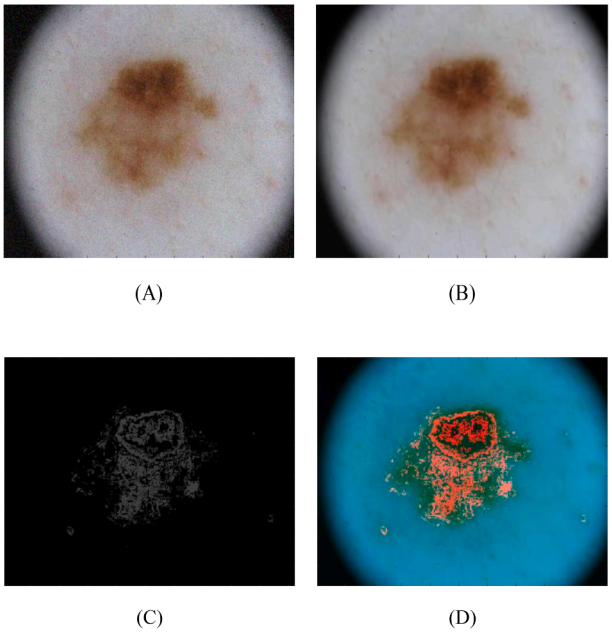

Fig. 2. A sample example for the skin cancer using the proposed approach: (A) Input Noisy image, (B) image after preprocessing, (C) image after segmentation by KFCM, (D) B + C.

$$Elongation = \frac{2\sqrt{Area}}{a\sqrt{\pi}} \tag{11}$$

$$Perimeter = \sum_{i=1}^{M}\sum_{j=1}^{N} b_p(i,j) \tag{12}$$

$$Variance = \frac{1}{MN}\sum_{i=1}^{M}\sum_{j=1}^{N}(p(i,j)-\mu) \tag{13}$$

$$Standarddeviation = \sqrt{Variance} \tag{14}$$

$$Irregularityindex = \frac{4\pi \times Area}{Perimeter^2} \tag{15}$$

$$Formfactor = \frac{Area}{a^2} \tag{16}$$

$$Eccentricity = 2a^{-1}\sqrt{(a^2-b^2)} \tag{17}$$

$$Energy = \sum_{i=1}^{M}\sum_{j=1}^{N} p^2(i,j) \tag{18}$$

$$Correlation = \sum_{i=1}^{M}\sum_{j=1}^{N}\frac{p(i,j)-\mu_r\mu_c}{\sigma_r\sigma_c} \tag{19}$$

$$\varphi_1 = \eta_{20}+\eta_{02}\varphi_2 = (\eta_{20}-\eta_{02})^2+4\eta_{11}^2\varphi_3 = (\eta_{30}-3\eta_{12})^2+(3\eta_{21}-\mu_{03})^2\varphi_4 = (\eta_{30}+3\eta_{12})^2+(3\eta_{21}+\mu_{03})^2 \tag{20}$$

where, b_p defines the boundary pixel's external side length, $p(i,j)$ represents the pixel intensity amount at the point (i, j), MN defines the image size, μ and σ demonstrate the average amount and the standard deviation value, orderly, and a and b are the major and the minor axis, respectively. After defining the features, some of the best ones should be selected optimally. The main task of feature selection method is to remove redundant features.

In this study, we used a metaheuristic-based feature selection methodology that is based on minimizing the following objective function:

$$Costfunction = \frac{(TP\times TN)-(FP\times FN)}{\sqrt{(TN+FP)\times(TP+FP)\times(TP+FN)\times(TN+FN)}} \tag{21}$$

where, TP, TN, FP, and FN represent Truly Positive, Truly Negative, False Positive, and False Negative, respectively.

For minimizing the above-mentioned objective function, we utilized a binarized and upgraded version of a recently proposed metaheuristic, named Arithmetic Optimization Algorithm for optimal selection of the features.

5. Developed Red fox Optimization (RFO) algorithm

5.1. The concept of optimization

Optimization means finding the best solution for a considered problem. This can be a quality or quantity concept [23]. In engineering problems, this term points to an approach to solve a mathematical objective function to find its optimum value that can be minimum or maximum based on our target [23,24]. Several works have been done on this subject [25]. For example, classic methods like gradient descent methods and the Pontryagin method provided the exact and optimal solution for these problems [23,26,27]. However, by increasing the complexity of these problems, the classic methods failed in solving the solution. Therefore, researchers focused on another kind of optimization solvers, called metaheuristics [28]. The metaheuristic algorithms are global solvers that can solve each type of optimization problem based on a stochastic solution with no needing for differentiation [29]. This made them an ideal solver in the recent engineering problems, especially, in medical imaging. The main idea of metaheuristics is inspired by nature, animal hunting behaviors, human beings, sports, etc. There are several types of these algorithms that are still increasing each year. For example, World Cup Optimization Algorithm (WCO) [30], Ant lion optimizer (ALO) algorithm [31], arithmetic optimization algorithm [32], and Tree Growth Algorithm (TGA) [33]. In this study, we will improve a newly introduced metaheuristic, called Developed Red Fox Optimization (RFO) Algorithm, to provide an optimal feature selection and an optimal classification strategy with combination by artificial neural network.

5.2. The Red fox Optimization (RFO) algorithm

Red foxes are carnivores with more or less slender and elongated bodies that are used to run fast and chase prey. Their heads are long and their ears are upright and pointed. They have a small size, with a head and body length of less than 80 cm and a shoulder height of less than 45 cm. It is of medium size and has a slender and elongated body, relatively short legs, and a hairy tail that comes in contact with the ground when the animal is standing. The folk of red foxes contains two kinds of lifestyles. One group is those living in a fixed and definite territory and the other group has a nomadic life. In both lifestyles, the leading of the crew is under the hierarchy of alpha couple. In these groups, after growing up the young foxes, can leave the group and form a new family and territory, or live with their parents and inherit the parent's territory for hunting. The main food of red foxes is small wild and domestic animals. This animal tries its chance to get food while crossing over the territory by hiding, close to the prey, and creeping up to the prey to giving an efficient attack. Fig. 3 shows the method of fox hunting modeling in the algorithm.

This algorithm, like any metaheuristic algorithm, has two main parts: territories' exploration, which models the prey selecting of the fox when it is distant from the prey, and the exploitation, that models the movement of fox for the closing to the prey as much as possible and to attack it. For initializing the algorithm, we need first to provide some randomly generated population candidates. By considering x as the initial population, we have:

$$\overline{x} = [x_0, x_1, \cdots, x_{n-1}] \tag{22}$$

For describing each fox x_i in iteration$t$, it is defined as $\left(\overline{x}_j^i\right)^t$, where i describes the population and j states the dimension of the problem in the research space. It is supposed that the candidates (foxes) move through

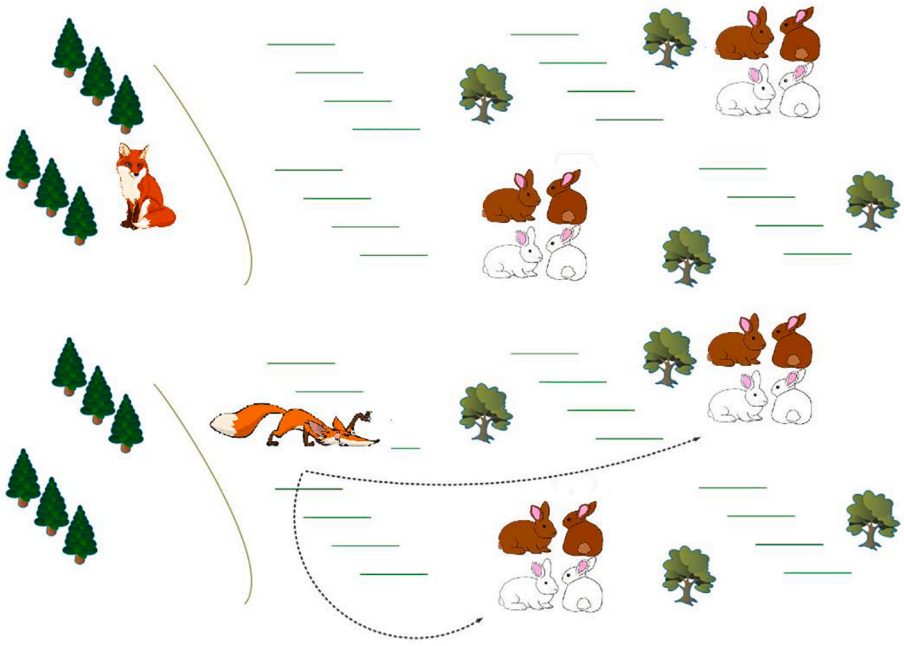

Fig. 3. Demonstrates the approach of fox hunting modeling in the algorithm.

solution space based on the equations. By considering $f \in R^n$ as the condition function of n variables, the following notation shows the points that are in the range $[a,b]^n$,

$$(\bar{x})^i = [(x_0)^i, (x_1)^i, \cdots, (x_{n-1})^i] \tag{23}$$

where $a,b \in R$.

So $(x)^i$ will be the best answer, when function $f\left((x)^i\right)$ gives the global optimum.

For global searching in the algorithm, the following rules are considered. In a flock of red foxes, each of them has their tasks to do to help the family in nature. If the territory has not had enough prey, the individuals go to distant places from their territory to find and to share it with the family. This is usually modeled by considering the fitness value of the candidates. In this regard, we sort population based on their fitness value, and for $\left(\bar{x}_{best}\right)^t$. To do so, the Euclidean distance square is achieved to the candidates as follows:

$$D\left(\left((\bar{x})^i\right)^t, \left(\bar{x}_{best}\right)^t\right) = \sqrt{\|\left((\bar{x})^i\right)^t - \left(\bar{x}_{best}\right)^t\|} \tag{24}$$

And then, the individuals move over the best solution by the following equation:

$$\left((\bar{x})^i\right)^t = \left((\bar{x})^i\right)^t + \alpha \times sgn\left(\left(\bar{x}_{best}\right)^t - \left((\bar{x})^i\right)^t\right) \tag{25}$$

where α is a randomly distributed value.

Here, if the new position has a better solution than the previous one, which will be selected as the new answer, else, the individuals will move back to the previous position. In this situation, if the explorers have found a proper position for hunting, they share the location information with the family, else, they will back with "empty hands''. It should note that due to being not familiar with the foxes in the distances, their ability to escape and hiding is less than their territory. This is modeled by eliminating the worst cases of the algorithm in each iteration.

The red fox crosses its areas in research of prey. If the fox observed its prey, it begins to approach silently, as close as possible, to avoid being seen. As a result, it circles and deceives the prey to show that it is not interested in hunting. When it approaches enough to the hunt, it runs as quickly as possible to get the prey. This process is considered as the exploitation searching part of the RFO algorithm. A random value, μ in the range [0,1] is employed for modeling the possibility of a fox being observed while getting nearer to the prey, such that:

$$\begin{cases} movecloserif\mu > 3/4 \\ stayandhideif\mu \le 3/4 \end{cases} \tag{26}$$

If during the iteration, μ indicates a movement to the population, a modified Cochleoid equation is used for visualizing the candidates' movement.

To consider the movement, the radius of the fox observation is considered by two parameters. The first parameter is a that describes a scaling parameter set for each candidate for randomly modeling the changing distance for approaching the prey. This parameter has a random amount in the area between 0 and 0.2. The second parameter is ϕ_0 that is employed for the candidates when the algorithm starts and models the angle of fox observation. This parameter is limited between 0 and 2π. With these two parameters, the vision radius of the hunting fox is achieved as follows:

$$r = \begin{cases} \dfrac{\mathrm{a} \times \sin(\phi_0)}{\phi_0} if\phi_0 \neq 0 \\ \gamma if\phi_0 = 0 \end{cases} \tag{27}$$

where γ shows a random amount in the interval [0, 1] that is taken as the adverse effect of weather conditions like rain and fog. And the movements of the candidates can be modeled based on the following equations:

$$\begin{cases} x_0^{New} = a \times r \times \cos(\phi_1) + x_0^{actual} \\ x_1^{New} = a \times r \times \sin(\phi_1) + a \times r \times \cos(\phi_2) + x_1^{actual} \\ x_1^{New} = a \times r \times \sin(\phi_1) + a \times r \times \sin(\phi_2) + a \times r \times \cos(\phi_3) + x_2^{actual} \\ \vdots \\ x_{n-1}^{New} = a \times r \times \sum_{k=1}^{n-2} \sin(\phi_1) + a \times r \times \cos(\phi_{n-1}) + x_{n-2}^{actual} \\ x_{n-1}^{New} = a \times r \times \sin(\phi_1) + a \times r \times \sin(\phi_2) + \cdots + a \times r \times \sin(\phi_{n-1}) + a \times r \times \sin(\phi_{n-1}) + x_{n-a}^{actual} \end{cases} \tag{28}$$

where, the angular values are randomized for the points based on $[\phi_1, \phi_2, \cdots \phi_{n-1}]$.

This models the fox behavior after it approaching the prey for hunting when it moves silently to the prey to attack the prey and its repetitive attempt to get another prey if it fails the first one. In the wild, the red fox must deal with various threats. Since there may be no food in the immediate habitat area, it may be essential for relocating. Humans are also a threat, as they will track down the fox if the fox does serious harm to a domestic animal population. Although, in the wild, foxes do not all die or migrate. The majority of them are highly intelligent and are capable of escaping and reproducing, supplying new lines to the fox herds.

For modeling this action, we chose five percent of the worst people in the society based on the criterion function's value, and this value is used as our personal opinion for simulating little variations in the flock in each iteration. We believe that these foxes either migrated elsewhere or were shot down by hunters because they are the least well-fitting. A model of habitat territory is used to develop by the alpha couple to replace them with new candidates to keep the population size constant. The best candidates have been selected $(\overline{x}(1))^t$ and $(\overline{x}(2))^t$ to denote the alpha couple in repetition t of the RFO algorithm, where, the habitat center is measured as follows:

$$(Hab^{center})^t = \frac{(\overline{x}(1))^t - (\overline{x}(2))^t}{2} \tag{29}$$

and the habitat diameter based on Euclidean distance is as follows:

$$\left(Hab^{diameter}\right)^t = \sqrt{\|(\overline{x}(1))^t - (\overline{x}(2))^t\|} \tag{30}$$

We select a random parameter, κ in the range [0, 1] during the iteration, that describes substitutes in the iteration based on the following equation:

$$\begin{cases} Newnomadiccandidateif \kappa > 0.45 \\ Reproductionofthealphacoupleif \kappa \leq 0.45 \end{cases} \tag{31}$$

New family members are initially believed to abandon the habitat as nomadic foxes in food search and the ability to reproduce in their flock.

Inside the research area, but outside the habitat, positions at random are selected. Then, the new candidates are created by the alpha pair, so we reproduce 2 of the best individuals $(\overline{x}(1))^t$ and $(\overline{x}(2))^t$ as a new candidate $((\overline{x}^{rep})^t)$.

$$(\overline{x}^{rep})^t = \kappa \frac{(\overline{x}(1))^t - (\overline{x}(2))^t}{2} \tag{32}$$

5.3. Developed Red fox Optimization (DRFO) algorithm

The RFO algorithm is one of the newest algorithms for optimization. However, it has several advantages and can be used for solving different kinds of problems, in some cases, it can result in a premature convergence. This can be observed in optimizing some objective functions in the default paper [34]. In recent years, several methods are introduced based on chaotic maps to improve the effectiveness of the metaheuristic algorithms [18].

As aforementioned, the parameter κ in the RFO algorithm has a random value, where, using during the iteration, the algorithm has a higher probability of premature convergence. In this research, a chaos mechanism based on circle mapping has been used for solving this problem. The mechanism maps the parameter κ into a regular formulation by the following equation [35]:

$$\kappa_{i+1} = \kappa_i + \beta - (\alpha - 2\pi) sin(2\pi\kappa_i) mod(1) \tag{33}$$

where, a chaotic time series $\kappa_i \in [0, 1]$ are generated by considering$\alpha = 0.5$ and $\beta = 0.2$ [35].

The study also used the Lévy flight (LF) technique to increase better convergence. The LF is a popular mechanism in metaheuristics [36]. These function models the random walk to controlling the local search by the following equation:

$$\mathrm{Le(w)} \approx \frac{1}{\mathrm{w}^{1+\tau}} \tag{34}$$

$$\mathrm{w} = \frac{\mathrm{A}}{|\mathrm{B}|^{1/\tau}} \tag{35}$$

$$\sigma^2 = \left\{ \frac{\Gamma(1+\tau)}{\tau\Gamma((1+\tau)/2)} \frac{\sin(\pi\tau/2)}{2^{(1+\tau)/2}} \right\}^{\frac{2}{\tau}} \tag{36}$$

where, $\Gamma()$ is the Gamma function, $\tau \in [0, 2]$ is the index of the LF mechanism (here, $\tau = 3/2$ [37]), and $A/B\ N(0, \sigma^2)$ represents that the samples are formed by a Gaussian distribution in which mean is zero and variance is σ^2, orderly.

By applying the LF mechanism, the new positions of the individuals are achieved as follows:

$$\left((\overline{x})^i\right)^t_{New} = \left((\overline{x})^i\right)^t + \alpha \times sgn\left(\left(\overline{x}_{best}\right)^t - \left((\overline{x})^i\right)^t\right) \times \mathrm{Le}(\delta) \tag{37}$$

5.4. Algorithm validation

This section will prove that why the proposed DRFO algorithm is a proper algorithm for feature selection than the other algorithms. For providing a guaranteed analysis, six different standard benchmark functions including two Unimodal 30-dimension functions, two Multimodal 30-dimension functions, and two Multimodal low dimension functions have been applied and their outcomes are compared with several new states of the art methods, including Locust Swarm Optimization (LS) [38], Multi-verse optimize (MVO) [39], Emperor penguin optimizer (EPO) [40], and the original Red Fox Optimization algorithm [34]. Simulation has been established under MATLAB R2019B environment that is based on the following configuration: Intel Core I7 laptop with 1.70 GHz speed and turbo boost up to 2.40 GHz and 16 GB of RAM. The simulation has been run 35 times independently for each

Table 1
The utilized benchmark functions and their desired values (f_{min}) and their constraint for the assessment [41].

Function	Range	f_{min}
$F_1(X) = \sum_{i=1}^{n-1}\left[100\left(x_{i+1}-x_i^2\right)^2+(x_i-1)^2\right]$	$[-30,30]^n$	0
$F_2(X) = \sum_{i=1}^{n-1}\left[(x_i+0.5)^2\right]$	$[-100,100]^n$	0
$F_3(X) = \sum_{i=1}^{n-1}\left(x_i^2-10\cos 2\pi x_i+10\right)$	$[-5.12,5.12]^n$	0
$F_4(X) = 0.1\left[\sin^2 3\pi x_1+\sum_{i=1}^{n}(x_i-1)^2\left(1+\sin^2(3\pi x_1+1)\right)+(x_n-1)^2\left(1+\sin^2(2\pi x_n)\right)\right]+\sum_{i=1}^{n}u(x_i,5,100,4)$	$[-50,50]^n$	0
$F_5(X) = \left(x_2-\frac{5.1}{4\pi^2}x_1^2+\frac{5}{n}x_1-6\right)^2+10\left(1-\frac{1}{8\pi}\right)\cos x_1+10$	$[-5,15]^2$	3979
$F_6(X) = -\sum_{i=1}^{4}c_i\exp\left(-\sum_{j=1}^{6}a_{ij}\left(x_j-p_{ij}\right)^2\right)$ $a_{ij}=\begin{pmatrix}10,3,17,3.5,1.7,8\\0.05,10,17,0.1,8,14\\3,3.5,1.7,10,17,8\\17,8,0.05,10,0.1,14\end{pmatrix}$, $c_i=[1,1.2,3,3.2]$	$[0,1]^6$	−3.32
$p_{ij}=\begin{pmatrix}0.1312,0.1696,0.5569,0.0124,0.8283,0.5886\\0.2329,0.4135,0.8307,0.3736,0.1004,0.9991\\0.2348,0.1415,0.3522,0.2883,0.3047,0.6650\\0.4047,0.8828,0.8732,0.5743,0.1091,0.0381\end{pmatrix}$		

Table 2
The parameter setting of the studied algorithms [42].

Algorithm	Parameter	Value
Locust Swarm Optimization (LS) [38]	F	0.6
	L	1
	g	20
Multi-verse optimize (MVO) [39]	Traveling distance rate	[0.6, 1]
	Wormhole existence prob.	[0.2, 1]
Emperor penguin optimizer (EPO) [40]	$\vec{A}$	[−1.5, 1.5]
	Temperature value ($T^{'}$)	[1, 1000]
	M	2
	f	[2, 3]
	S	[0, 1.5]
	l	[1.5, 2]
Red Fox Optimization (RFO) [34]	a	0.2
	ϕ_0	1

algorithm and function to provide reliable results for comparison. Table 1 tabulates the utilized benchmark functions and their desired values (f_{min}) and their constraint for the assessment [41].

To provide a fair comparison, the population for whole of the algorithms is set at 80 with 400 iterations for all of them. Table 2 indicates the parameter setting of the studied algorithms [42].

Simulation results of the analysis are tabulated in Table 3. This analysis is using considering the mean value (mean), the minimum value (min) and the variance (Var).

According to the results in Table 3, the proposed DRFO algorithm provides the best minimum values for the studies' benchmark functions for both mean value and minimum value. This shows the higher accuracy of the method in finding the solution.

To show the system processing speed, its running time is also compared with the compared methods. Fig. 4 shows this comparison.

As can be observed, the proposed DRFO method has a good execution time for solving the analyzed functions, however, due to using the developed version, the running time is more than EPO which is because of its better accuracy that this algorithm. As can be seen, the main advantage of the proposed DRFO algorithm is to provide a proper trade-off between the accuracy and the precision which is important for our purpose.

Also, it can be observed that the standard deviation (Var) of the proposed DRFO algorithm is the minimum against the others that shows its higher consistency in finding reliable solutions. To this end, a logistic function transformation $S\left((\overline{x})^i\right)^t$ has been utilized:

$$S\left((\overline{x})^i\right)^t = Sigmoid\left((\overline{x})^i\right)^t = \frac{1}{1+e^{-\left((\overline{x})^i\right)^t}} \tag{38}$$

If $rnd < S\left((\overline{x})^i\right)^{t+1}$, then $\left((\overline{x})^i\right)^t = 1$

Else, $\left((\overline{x})^i\right)^{t+1} = 0$where, $S\left((\overline{x})^i\right)^t$ describes a sigmoid limiting transformation and *rnd* defines a quasi-random number selected by a uniform distribution in the interval [0.1, 1].

Table 3
Comparison results of the analysis performed on the studied benchmark functions.

Function	Metric	LS [38]	MVO [39]	EPO [40]	RFO [34]	DRFO
F_1	Mean	1.21E+3	3.85E+4	61.41	48.73	36.03
	Min	218.41	150.74	53.38	25.18	19.24
	Var	4.24E+5	3.04E+5	2.17E+5	0.65	0.51
F_2	Mean	28.65	1.85E−3	2.97	2.16	0
	Min	18.63	1.71E−4	0.68	0.57	0
	Var	30.01	1.85E−4	10.012	8.83	0
F_3	Mean	0.529	0.86	0.56	3.14E−3	4.95E−4
	Min	0.416	0.625	0.404	2.89E−4	3.97E−5
	Var	1.93E−3	2.75E−3	6.28E−3	4.23E−7	4.91E−8
F_4	Mean	0.122	0.086	2.81E−3	5.16E−6	3.45E−18
	Min	0.073	0.055	4.13E−5	3.89E−7	2.46E−18
	Var	8.08E−4	6.39E−4	7.00E−6	8.64E−8	3.31E−20
F_5	Mean	0.64	0.64	0.64	0.64	0.64
	Min	0.64	0.64	0.64	0.64	0.64
	Var	1.53E−8	6.47E−10	5.79E−11	4.18E−12	6.35E−14
F_6	Mean	−5.43	−5.29	−5.18	−4.56	−3.75
	Min	−4.65	−4.52	−4.49	−4.39	−4.39
	Var	2.43E−3	2.33E−3	1.72E−3	1.53E−3	1.25E−3

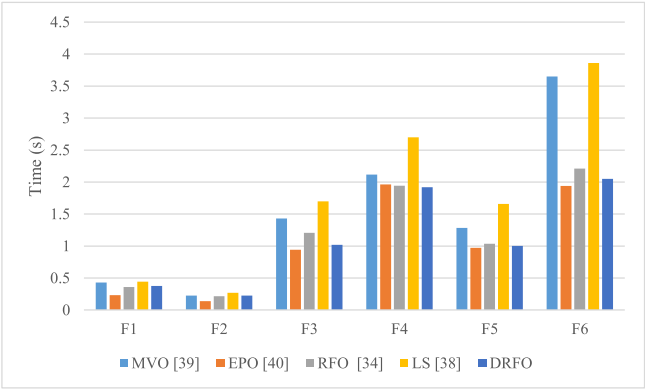

Fig. 4. The execution time for the DRFO algorithm compared with the other analyzed methods.

6. Classification based on optimized DRFO

After features selection, it is needed to use a classifier to give the final classification of the system. Here, a new optimized version of multilayer perceptron (MLP) is utilized [42]. The MLPs are efficient methods for solving complicated and nonlinear problems. It makes an appropriate relationship between the input and the output data with a low sensitivity against the errors [43]. Therefore, this method is utilized here for accurate classification of the melanoma images by providing correct training with no mathematical modeling [44,45].

This network contains a model with several numbers of biases and weights which are in a strong interconnection with each other to get better performance of the brain. The MLP uses a widely-used method, backpropagation (BP) for minimization of the network error. Based on the BP method, the value of the biases and weights are tuned to minimize the error between the desired value and the output value. This is done by utilizing the Gradient Descent (GD) algorithm. A noteworthy problem of the GD is that it can be easily trapped into the local minimum. The output of the layers in the network is mathematically formulated as follows:

$$z_i = \sum_{j=1}^{n} w_{ij}\alpha_i + b_j \tag{39}$$

where, α_i describes the i^{th} input variable, w_{ij} signifies the relation weight between α_i and the j^{th} invisible neuron, and b_j defines the j^{th} bias

The activation function used in this study is sigmoid that is achieved by the following:

$$f_j(z) = \frac{1}{1+e^{-z_j}} \tag{40}$$

And the output layer is obtained by the following:

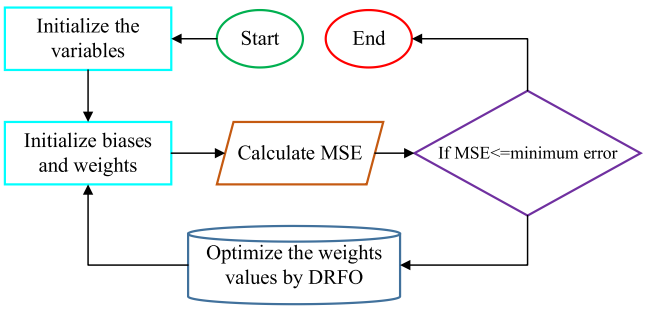

Fig. 5. The block diagram of the proposed classification strategy.

$$y_i = \sum_{j=1}^{m} w_{kj}\alpha_i + \beta_k \tag{41}$$

The MLP evaluates Mean square error (MSE) between the observed output and the desired output as follows:

$$MSE = \frac{1}{n} \times \sum\nolimits_{i=1}^{n} y_i - d_i \tag{42}$$

where, n represents the iteration number of the training data collection, and d_i and y_i describe the desired value and the observed value, respectively.

Based on the beforementioned explanations, to resolve the GD problems in MLP, the proposed DRFO algorithm is used to minimize the MSE of the network to provide an optimized classifier. Fig. 5 shows the block diagram of the proposed classification strategy.

The final optimum features for optimization are: *Rectangularity* , *Entropy*, *Homogeneity*, *Elongation*, *Irregularityindex*, *Correlation*, φ_1, φ_2. Therefore, the number of features after feature selection is 8.

7. Simulation results

The purpose of this paper is to introduce a new optimized pipeline methodology for melanoma diagnosis from dermoscopy images. The idea is to provide a newly designed metaheuristic to get a method with lower complexity (feature selection part) and higher accuracy (classification part). To validate the proposed method, it has been performed on the ISIC 2020 database and its results have been compared with some other state-of-the-art methods.

7.1. ISIC challenge dataset

For validating the presented melanoma detection system, the Skin Imaging Collaboration (ISIC) database is utilized. The ACS database includes 13,000 dermoscopic images which are extracted from the Nevoscope system which is sponsored by the International Society for Digital Imaging of the Skin (ISDIS). Most images have linked clinical metadata, which has been vetted by recognized melanoma experts. Fig. 6 shows some examples from the ISIC 2020 dataset as lesion images and their ground truths. This dataset can be downloaded from: https://challenge.isic-archive.com/data#2016.

The pipeline procedure of the proposed method is shown in Fig. 7.

7.2. Results

In the present investigation, 90 % of the data are utilized to train the classifier and the remained 10 % are used for testing the data. To form a machine learning model with the data from dataset, the data has been splitted into training and validation/test sets. The training set has been employed to train the model, and the validation/test set has been employed to validate it on data it has never seen before. The approach is to do a simple 90%-10% split [46].

The network has been trained by 850 iterations and 30 times run independently and their average value is used to accomplish a suitable result. To determine the higher superiority of the optimized classifier than the original ANN, its Receiver Operating Characteristic (ROC) curve is compared with the ANN. The ROC curve illustrates a graphical profile that indicates the diagnostic ability of a binary classifier system as its discrimination threshold is changed. The ROC curve of the proposed method compared with some state-of-the-art methods, including dE-ANN [47], BUZO [48], ANN [49], ANN-WCO [50], SVM-FSO [51], Jiannai's Deep [52], and Deep-PSO [53] are shown in Fig. 8.

In the ROC curve, the vertical axis and the horizontal axis show the sensitivity and the specificity, respectively. As shown in Fig. 8, the proposed ANN-WCO classifier provides a higher Area Under the Curve (AUC) value (0.83) compared with that in the original ANN model

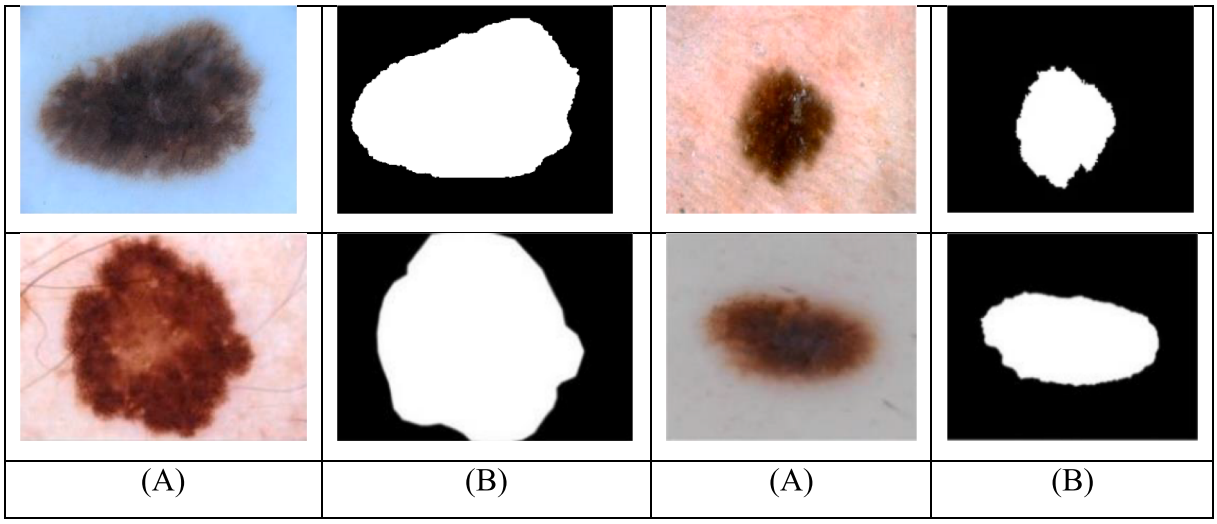

Fig. 6. Some skin lesion examples and their ground truths from ISIC 2020 dataset: (A) dermoscopic image sample and (B) its binary ground truth from the ISIC 2020 dataset.

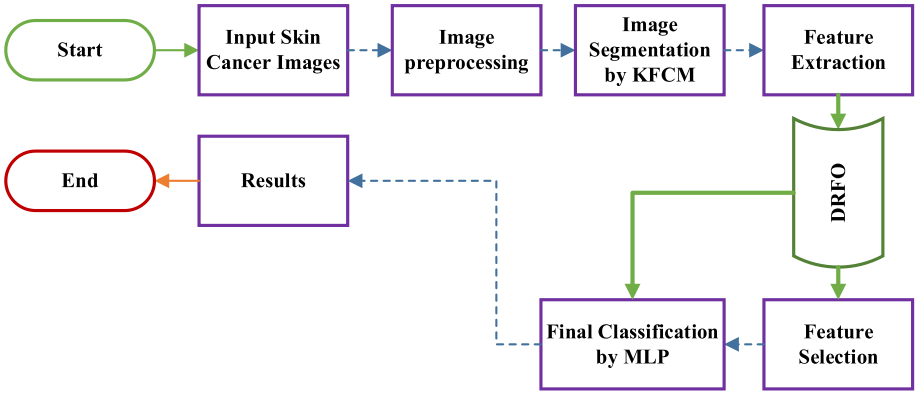

Fig. 7. The pipeline procedure of the proposed method.

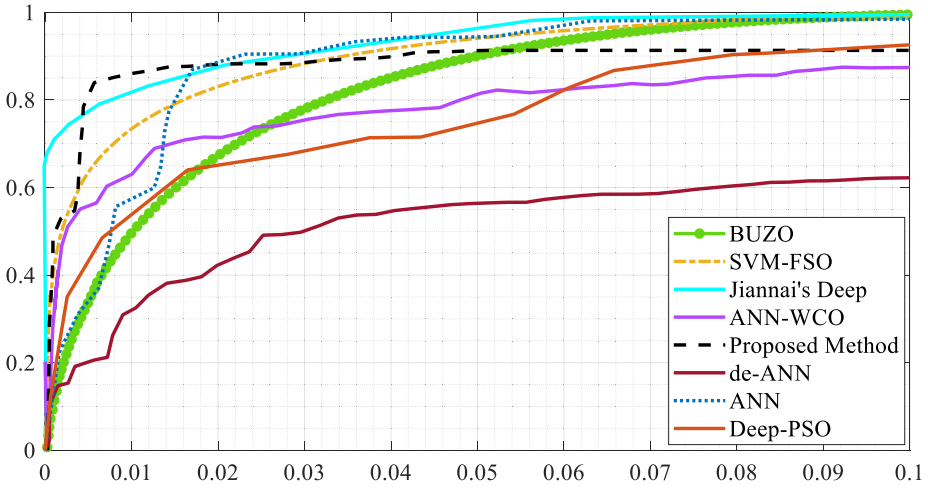

Fig. 8. ROC curve of the MLP classifier.

(0.75). This proves the superior efficiency of the ANN-WCO model compared with the ANN model.

For analyzing the system, four measurement indicators including Jaccard Index, specificity, accuracy, and sensitivity have been used that are formulated below:

$$J(A,B) = \frac{|A \bigcap B|}{|A \bigcup B|} \tag{43}$$

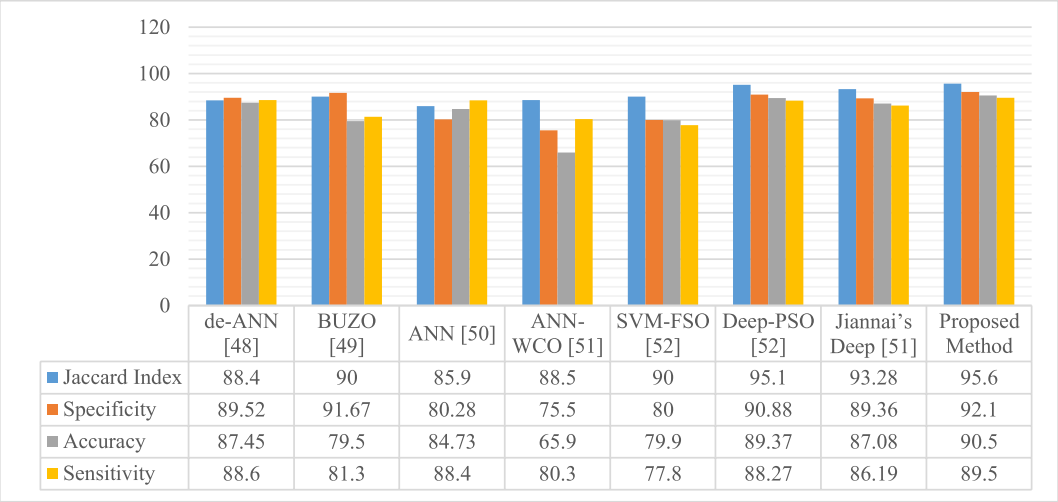

	de-ANN [48]	BUZO [49]	ANN [50]	ANN-WCO [51]	SVM-FSO [52]	Deep-PSO [52]	Jiannai's Deep [51]	Proposed Method
Jaccard Index	88.4	90	85.9	88.5	90	95.1	93.28	95.6
Specificity	89.52	91.67	80.28	75.5	80	90.88	89.36	92.1
Accuracy	87.45	79.5	84.73	65.9	79.9	89.37	87.08	90.5
Sensitivity	88.6	81.3	88.4	80.3	77.8	88.27	86.19	89.5

Fig. 9. Shows the statistical experiment results.

$$Specificity = \frac{TN}{\mathrm{TN} + \mathrm{FP}} \tag{44}$$

$$Accuracy = \frac{TP + TN}{TP + TN + FP + FN} \tag{45}$$

$$Sensitivity = \frac{TP}{TP + FN} \tag{46}$$

where, TP, TN, FP, and FN show the truly positive, true negative, false positive, and false negative. For providing a fair analysis of the proposed technique, its results are compared with some state-of-the-art methods, including dE-ANN [47], BUZO [48], ANN [49], ANN-WCO [50], SVM-FSO [51], Jiannai's Deep [52], and Deep-PSO [53]. Fig. 9 illustrates the validation outcomes of the studied methods.

It is observed from Fig. 8 that, the suggested methodology with 90.5% accuracy provides the highest accuracy among the other comparative methods. The method with 92.1 % Specificity and 89.5 % sensitivity, has also proper reliability against the others. Based on Jaccard Index that is achieved 95.6 % for the proposed method, it shows that how far there is a conjunction between the ground real images and the segmented images, and also the deviation is estimated. Therefore, the method provided the best results than the others as a diagnosis system.

8. Conclusions

Skin cancer, particularly melanoma, describes one of the most common cancers. Early detection of this cancer is too helpful to cure it. In this research, a new optimal computer-aided design was presented for the accurate diagnosis of melanoma from dermoscopy images. The output of the design splits the input data into two clusters, healthy and cancerous cases. Here, image preprocessing was first based on median filtering. Median filtering was utilized for removing the noise of the input images. Then, to determine the region of interest in the images, the Kernel Fuzzy C-means method was utilized. The idea of using Kernel Fuzzy C-means was that it is favored by researchers in practical applications, and has gradually formed a complete theoretical system over continuous application and research. The main features of the segmented area were then optimally extracted and selected, and finally, an optimized classification method based on multi-layer perceptron was used for the diagnosis of the images. To provide an optimized version of feature selection and image classification, a newly developed version of the Red Fox Optimization (DRFO) Algorithm was utilized. The optimization method was used for increasing the accuracy and the consistency of the original algorithm. The main advantage of using this algorithm was that improved the classification accuracy and the shortcoming of this study is that due to using additional improvement, the complexity of the method was increased. Simulations results performed on the ISIC 2020 database were compared with some famous approaches to prove the efficacy of the approach on the way to the others. The results showed that the proposed method with 90.5% accuracy provides the highest accuracy among the others. Also, the proposed method with 92.1% Specificity and 89.5% sensitivity, delivers suitable reliability toward the others. Furtheremore, by analyzing the method performance basd on Jaccard Index, 95.6 % efficiency was achieved for the proposed method which showed how far there is a conjunction between the ground real images and the segmented images, and also the deviation is estimated. In the future work, we will work on using an adaptive optimization technique to improve the method to reduce the method complexity in the time viewpoint.

CRediT authorship contribution statement

Zexian Fu: Conceptualization, Data curation, Writing - original draft, Writing - review & editing. **Jing An:** Conceptualization, Data curation, Writing - original draft, Writing - review & editing. **Qiuyu Yang:** Conceptualization, Data curation, Writing - original draft, Writing - review & editing. **Haojun Yuan:** Conceptualization, Data curation, Writing - original draft, Writing - review & editing. **Yuhang Sun:** Conceptualization, Data curation, Writing - original draft, Writing - review & editing. **Homayoun Ebrahimian:** Conceptualization, Data curation, Writing - original draft, Writing - review & editing.

Declaration of Competing Interest

The authors declare that they have no known competing financial interests or personal relationships that could have appeared to influence the work reported in this paper.

References

[1] Z. Xu, et al., Computer-aided diagnosis of skin cancer based on soft computing techniques, Open Med. 15 (1) (2020) 860–871.
[2] G. Guo, N. Razmjooy, A new interval differential equation for edge detection and determining breast cancer regions in mammography images, Syst. Sci. Control Eng. 7 (1) (2019) 346–356.
[3] N. Razmjooy, M. Ramezani, N. Ghadimi, Imperialist competitive algorithm-based optimization of neuro-fuzzy system parameters for automatic red-eye removal, Int. J. Fuzzy Syst. 19 (4) (2017) 1144–1156.
[4] M. Gheydi, A. Nouri, N. Ghadimi, Planning in microgrids with conservation of voltage reduction, IEEE Syst. J. 12 (3) (2018) 2782–2790.

[5] A. Seal, D. Bhattacharjee, M. Nasipuri, Predictive and probabilistic model for cancer detection using computer tomography images, Multimedia Tools Appl. 77 (3) (2018) 3991–4010.

[6] N. Razmjooy, M. Ashourian, M. Karimifard, V.V. Estrela, H.J. Loschi, D. do Nascimento, R.P. França, M. Vishnevski, Computer-aided diagnosis of skin cancer: a review, Curr. Med. Imaging 16 (7) (2020) 781–793.

[7] F.R.S. Navid Razmjooy, Noradin Ghadimi, A hybrid neural network – world cup optimization algorithm for melanoma detection, Open Med. 13 (2018) 9–16.

[8] Q. Liu, Z. Liu, S. Yong, K. Jia, N. Razmjooy, Computer-aided breast cancer diagnosis based on image segmentation and interval analysis, Automatika 61 (3) (2020) 496–506.

[9] N. Razmjooy, V.V. Estrela, H.J. Loschi, Entropy-based breast cancer detection in digital mammograms using world cup optimization algorithm, Int. J. Swarm Intell. Res. 11 (3) (2020) 1–18.

[10] A. Costa, Y. Kieffer, A. Scholer-Dahirel, F. Pelon, B. Bourachot, M. Cardon, P. Sirven, I. Magagna, L. Fuhrmann, C. Bernard, C. Bonneau, M. Kondratova, I. Kuperstein, A. Zinovyev, A.-M. Givel, M.-C. Parrini, V. Soumelis, A. Vincent-Salomon, F. Mechta-Grigoriou, Fibroblast heterogeneity and immunosuppressive environment in human breast cancer, Cancer Cell 33 (3) (2018) 463–479.e10.

[11] E. Somfai, et al., Minimizing false negative rate in melanoma detection and providing insight into the causes of classification. arXiv preprint arXiv: 2102.09199, 2021.

[12] P. Bansal, et al., Using transfer learning and hierarchical classifier to diagnose melanoma from dermoscopic images, Int. J. Healthcare Inf. Syst. Inf. 16 (2) (2021) 73–86.

[13] T. Fan, et al., Identification of skin melanoma based on microscopic hyperspectral imaging technology, in: Twelfth International Conference on Signal Processing Systems. 2021. International Society for Optics and Photonics.

[14] E. Vocaturo, E. Zumpano, Useful features for computer-aided diagnosis systems for melanoma detection using dermoscopic images, in: Handbook of Research on Automated Feature Engineering and Advanced Applications in Data Science, 2021, IGI Global. pp. 48–71.

[15] N. Dey, et al., A study on the bat algorithm technique to evaluate the skin melanoma images, in: Applications of Bat Algorithm and its Variants, 2021, Springer, pp. 45–60.

[16] P. Akbary, M. Ghiasi, M.R.R. Pourkheranjani, H. Alipour, N. Ghadimi, Extracting appropriate nodal marginal prices for all types of committed reserve, Comput. Econ. 53 (1) (2019) 1–26.

[17] K.-S. Kim, et al., Improved simple linear iterative clustering superpixel. 2013 IEEE International Symposium on Consumer Electronics (ISCE), IEEE, 2013.

[18] A.K. Gupta, A. Seal, P. Khanna, Divergence based SLIC, Electron. Lett. 55 (14) (2019) 783–785.

[19] C. Panigrahy, A. Seal, N.K. Mahato, Fractal dimension of synthesized and natural color images in lab space, Pattern Anal. Appl. 23 (2) (2020) 819–836.

[20] A. Karlekar, A. Seal, O. Krejcar, C. Gonzalo-Martin, Fuzzy k-means using non-linear s-distance, IEEE Access 7 (2019) 55121–55131.

[21] A. Seal, et al., Fuzzy c-means clustering using Jeffreys-divergence based similarity measure, Appl. Soft Comput. 88 (2020), 106016.

[22] M.R.P. Ferreira, F.d.A.T. de Carvalho, Kernel fuzzy c-means with automatic variable weighting, Fuzzy Sets Syst. 237 (2014) 1–46.

[23] N. Ghadimi, A. Afkousi-Paqaleh, A. Emamhosseini, A PSO-based fuzzy long-term multi-objective optimization approach for placement and parameter setting of UPFC, Arab. J. Sci. Eng. 39 (4) (2014) 2953–2963.

[24] H. Ebrahimian, S. Barmayoon, M. Mohammadi, N. Ghadimi, The price prediction for the energy market based on a new method, Econ. Res.-Ekonomska istraživanja 31 (1) (2018) 313–337.

[25] D. Yu, et al., Energy management of wind-PV-storage-grid based large electricity consumer using robust optimization technique, J. Storage Mater. 27 (2020), 101054.

[26] J. Liu, C. Chen, Z. Liu, K. Jermsittiparsert, N. Ghadimi, An IGDT-based risk-involved optimal bidding strategy for hydrogen storage-based intelligent parking lot of electric vehicles, J. Storage Mater. 27 (2020) 101057, https://doi.org/10.1016/j.est.2019.101057.

[27] M. Saeedi, M. Moradi, M. Hosseini, A. Emamifar, N. Ghadimi, Robust optimization based optimal chiller loading under cooling demand uncertainty, Appl. Therm. Eng. 148 (2019) 1081–1091.

[28] Q. Meng, T. Liu, C. Su, H. Niu, Z. Hou, N. Ghadimi, A single-phase transformer-less grid-tied inverter based on switched capacitor for PV application, J. Control Autom. Electr. Syst. 31 (1) (2020) 257–270.

[29] Z. Yuan, W. Wang, H. Wang, N. Ghadimi, Probabilistic decomposition-based security constrained transmission expansion planning incorporating distributed series reactor, IET Gener. Transm. Distrib. 14 (17) (2020) 3478–3487.

[30] M. Dehghani, M. Ghiasi, T. Niknam, A. Kavousi-Fard, M. Shasadeghi, N. Ghadimi, F. Taghizadeh-Hesary, Blockchain-based securing of data exchange in a power transmission system considering congestion management and social welfare, Sustainability 13 (1) (2021) 90, https://doi.org/10.3390/su13010090.

[31] M. Mani, O. Bozorg-Haddad, X. Chu, Ant lion optimizer (ALO) algorithm, in: Advanced Optimization by Nature-Inspired Algorithms, Springer, 2018, pp. 105–116.

[32] L. Abualigah, et al., The arithmetic optimization algorithm, Comput. Methods Appl. Mech. Eng. 376 (2021), 113609.

[33] A. Cheraghalipour, M. Hajiaghaei-Keshteli, M.M. Paydar, Tree Growth Algorithm (TGA): a novel approach for solving optimization problems, Eng. Appl. Artif. Intell. 72 (2018) 393–414.

[34] D. Połap, M. Woźniak, Red fox optimization algorithm, Expert Syst. Appl. 166 (2021), 114107.

[35] R.C. Hilborn, Chaos and nonlinear dynamics: an introduction for scientists and engineers, 2000, Oxford University Press on Demand.

[36] C. Choi, J.-J. Lee, Chaotic local search algorithm, Artif. Life Robot. 2 (1) (1998) 41–47.

[37] X. Li, P. Niu, J. Liu, Combustion optimization of a boiler based on the chaos and Levy flight vortex search algorithm, Appl. Math. Model. 58 (2018) 3–18.

[38] E. Cuevas, F. Fausto, A. González, The locust swarm optimization algorithm, in: New Advancements in Swarm Algorithms: Operators and Applications, Springer, 2020, pp. 139–159.

[39] S. Mirjalili, S.M. Mirjalili, A. Hatamlou, Multi-verse optimizer: a nature-inspired algorithm for global optimization, Neural Comput. Appl. 27 (2) (2016) 495–513.

[40] G. Dhiman, V. Kumar, Emperor penguin optimizer: a bio-inspired algorithm for engineering problems, Knowl.-Based Syst. 159 (2018) 20–50.

[41] C. Chen, S. Wang, X. Wang, H. Yu, R. Dong, Improved fluid search optimization-based real-time weed mapping, Inf. Process. Agric. 7 (3) (2020) 403–417.

[42] Z. Yang, M. Ghadamyari, H. Khorramdel, S.M. Seyed Alizadeh, S. Pirouzi, M. Milani, F. Banihashemi, N. Ghadimi, Robust multi-objective optimal design of islanded hybrid system with renewable and diesel sources/stationary and mobile energy storage systems, Renew. Sustain. Energy Rev. 148 (2021) 111295, https://doi.org/10.1016/j.rser.2021.111295.

[43] M. Mehrpooya, N. Ghadimi, M. Marefati, S.A. Ghorbanian, Numerical investigation of a new combined energy system includes parabolic dish solar collector, Stirling engine and thermoelectric device, Int. J. Energy Res. 45 (11) (2021) 16436–16455.

[44] Haixiong Ye, et al., High step-up interleaved dc/dc converter with high efficiency, Energy Sour. Part A (2020) 1–20.

[45] X. Fan, H. Sun, Z. Yuan, Z. Li, R. Shi, N. Ghadimi, High voltage gain DC/DC converter using coupled inductor and VM techniques, IEEE Access 8 (2020) 131975–131987.

[46] B.M. NEGASH, A.D. YAW, Artificial neural network based production forecasting for a hydrocarbon reservoir under water injection, Pet. Explor. Dev. 47 (2) (2020) 383–392.

[47] M. Kumar, M. Alshehri, R. AlGhamdi, P. Sharma, V. Deep, A de-ann inspired skin cancer detection approach using fuzzy c-means clustering, Mobile Networks Appl. 25 (4) (2020) 1319–1329.

[48] A. Arshaghi, M. Ashourian, L. Ghabeli, Detection of Skin Cancer Image by Feature Selection Methods Using New Buzzard Optimization (BUZO) Algorithm, Traitement du Signal 37 (2) (2020) 181–194.

[49] J.A. Jaleel, S. Salim, R. Aswin, *Artificial neural network based detection of skin cancer*, Int. J. Adv. Res. Electr. Electron. Instrum. Eng. 1 (3) (2012).

[50] F. Mirzapour, M. Lakzaei, G. Varamini, M. Teimourian, N. Ghadimi, A new prediction model of battery and wind-solar output in hybrid power system, J. Ambient Intell. Humanized Comput. 10 (1) (2019) 77–87.

[51] M. Li, C. Han, F. Fahim, Skin cancer diagnosis based on support vector machine and a new optimization algorithm, J. Med. Imag. Health Inf. 10 (2) (2020) 356–363.

[52] S. Jinnai, N. Yamazaki, Y. Hirano, Y. Sugawara, Y. Ohe, R. Hamamoto, The development of a skin cancer classification system for pigmented skin lesions using deep learning, Biomolecules 10 (8) (2020) 1123, https://doi.org/10.3390/biom10081123.

[53] T.Y. Tan, L. Zhang, C.P. Lim, Intelligent skin cancer diagnosis using improved particle swarm optimization and deep learning models, Appl. Soft Comput. 84 (2019), 105725.